

Analysis of luminosity measurements of the pre-white dwarf PG 1159-035: an approach featuring a dynamical database

E. Matsinos*

*Electronic mail: evangelos (dot) matsinos (at) sunrise (dot) ch

Abstract

In a previous work, those of the luminosity measurements of the pre-white dwarf PG 1159-035 which are available online yielded estimates for the optimal embedding dimension, for the dimensionality of the phase space reconstructed from these observations, and for the maximal Lyapunov exponent λ : the result $\lambda = (9.2 \pm 1.0(\text{stat.}) \pm 2.7(\text{syst.})) \cdot 10^{-2} \Delta\tau^{-1}$ ($\Delta\tau = 10$ s is the sampling interval in the measurements) was obtained, suggesting that the physical processes, underlying the variation of the luminosity of PG 1159-035, are chaotic.

An improved approach is employed in the present work in relation to the database of embedding vectors: instead of assigning each of the input time-series arrays either to the training or to the test set, the new approach features the creation of a dynamical database, i.e., of one which depends on the choice of the input test file. Although the size of the database is thus increased by a factor of about 2 (compared to the previous study), the impact of this change on the important results is found to be insignificant. The estimate of this work for the maximal Lyapunov exponent ($\lambda = (8.9 \pm 0.7(\text{stat.}) \pm 1.9(\text{syst.})) \cdot 10^{-2} \Delta\tau^{-1}$) is in very good agreement with the result of the earlier study.

PACS 2010: 05.10.-a; 05.45.-a; 05.45.Gg; 45.30.+s; 95.10.Fh

Key words: Statistical Physics and Nonlinear Dynamics; Linear/Nonlinear Dynamical Systems; Applications of Chaos; Chaos Astronomy

1 Introduction

Reported in Ref. [1] were the results of an analysis of those of the luminosity measurements of the pre-white dwarf PG 1159-035 which had found their way into the ‘Time-series data source Archives: Santa Fé Time Series Competition’ database [2]. The seventeen time-series arrays of Ref. [2] (to be called ‘original’ from now on) appear to be snippets of the data acquired in the Whole

Earth Telescope (WET) project in 1989. The rich power spectrum of the detected radiation was explored in Refs. [3,4], resulting in the identification of 198 pulsation modes of this celestial body. Also extracted in Refs. [3,4] was accurate information on the important physical properties of PG 1159-035, i.e., its rotation period, mass, magnetic field, and structure.

The original time-series arrays were band-passed in Ref. [1], using an elliptical filter and the band-pass corner frequencies of 1 and 3 mHz, which (according to Refs. [3,4]) delimit the region of interest in the power spectrum of PG 1159-035 as far as the non-radial gravity-wave (g -wave) pulsations of this celestial body are concerned. In Ref. [1], the filtered data was split into two parts of comparable sizes, one yielding the training (learning) set or database, the other the test set. The optimal embedding dimension m_0 was subsequently determined using Cao's method [5]: Cao's $E1$, representing the relative change of the average distance between neighbouring embedding vectors when increasing the embedding dimension by one unit, appeared to saturate in the vicinity of 10, a result for m_0 which was corroborated by an analysis of the correlation dimension.

The extraction of the maximal Lyapunov exponent λ , characterising the rapidity of the exponential divergence between predictions and observations in chaotic systems, was subsequently pursued, by fitting a monotonic function to the out-of-sample prediction-error arrays $S(k)$. The original $S(k)$ arrays contain sizeable undulations, which hinder the establishment of the region in the $(k, S(k))$ plane within which a linear relationship (i.e., the signature of a chaotic dynamical system) holds. Parenthetically, a modification in the evaluation of the $S(k)$ arrays was put forward in Ref. [1], after introducing a weight which depends on the distance between two embedding vectors contributing to $S(k)$.

An estimate for the maximal Lyapunov exponent λ was obtained for embedding dimensions m between 10 and 12, within the domain of neighbourhood sizes ϵ for which a linear relationship with the correlation sums $C(\epsilon)$ (on a log-log plot) could be established: the final result $\lambda = (9.2 \pm 1.0(\text{stat.}) \pm 2.7(\text{syst.})) \cdot 10^{-2} \Delta\tau^{-1}$ was obtained, where $\Delta\tau$ is the sampling interval in the measurements, namely 10 s. Therefore, the findings of Ref. [1] suggest that the physical processes, underlying the variation of the luminosity of PG 1159-035, are chaotic.

Two reasons call for further analysis of these measurements. The first one relates to the filtering of the original time-series arrays; this modification is expected to have a minor impact. The second reason relates to the creation of the database of embedding vectors; the significance of the impact of this modification on the important results of the study needs to be assessed.

- In Ref. [1], the filtering of the original time-series arrays was performed ‘left-to-right’ (i.e., following the arrow of time). On the contrary, the original arrays will be subjected to a symmetrical, two-sided filtering in this work. This procedure has two advantages: first, it is expected to lead to the reduction of transient effects (which are due to the application of an IIR digital filter) at the start of each filtered array; second, it is expected to reduce the delay between the original and the filtered data. The elliptical filter of Ref. [1] will be applied herein to the original time-series arrays, ‘left-to-right’ and ‘right-to-left’. The output of the filtering procedure will be the average of the two filtered forms.
- In Ref. [1], the training and test sets were fixed at the outset of the study: each of the (filtered) time-series arrays was assigned to one of the two sets, and remained in that set throughout the analysis. The procedure, put forward in Ref. [1] for the determination of these two sets, led to the assignment of 12617 measurements to the former set and of 14574 to the latter. Despite the fact that the splitting of the data into (fixed) training and test sets is an efficient way in suppressing the effects of the temporal correlations¹, alternative analysis options, which are equally promising in terms of the suppression of these effects, are worth investigating (at least, for the sake of comparison and verification of the important results). One such possibility, featuring the creation of a dynamical database, is explored in this work (see Section 3).

Apart from these two changes, the reader is addressed to Ref. [1] for a concise description of the theoretical background upon which the study rests, as well as for other important details on the analysis.

2 The filtering of the time-series arrays of Ref. [2]

The original time-series arrays were submitted to the two-sided filtering procedure as described in the introduction. Some of the properties of the resulting filtered arrays are given in Table 1. The values of the embedding delay ν come out consistent after the filtering, namely either 13 or 14 sampling intervals in all cases. Equally comforting is the assertion of the stationarity of the observations, as revealed by the p-values, which exceed the threshold of statistical significance p_{\min} assumed in this work (as in Ref. [1], $p_{\min} = 1.00 \cdot 10^{-2}$).

¹ As the original time-series arrays of Ref. [2] had obviously been obtained from a pool of measurements containing at least three times the amount of the chosen data, it is reasonable to assume that the data sets of Ref. [2] are independent (i.e., no set contains elements which are temporally correlated with any of the elements of any other set).

Table 1

Some properties of the filtered time-series arrays of PG 1159-035; s stands for ‘signal’ and represents the values of each array. The original measurements were subjected to a two-sided filtering, using the elliptical filter which had been applied to the data (‘left-to-right’) in Ref. [1].

Data set	s_{\min}	s_{\max}	$s_{\max} - s_{\min}$	$\langle s \rangle$	rms	p-value	ν
E01	-0.2232	0.2314	0.4546	$3.026 \cdot 10^{-4}$	$1.083 \cdot 10^{-1}$	$9.35 \cdot 10^{-1}$	14
E02	-0.1823	0.1774	0.3596	$-4.645 \cdot 10^{-5}$	$7.128 \cdot 10^{-2}$	$9.26 \cdot 10^{-1}$	14
E03	-0.1257	0.1261	0.2518	$1.018 \cdot 10^{-4}$	$6.292 \cdot 10^{-2}$	$9.28 \cdot 10^{-1}$	13
E04	-0.1393	0.1221	0.2614	$1.210 \cdot 10^{-4}$	$6.489 \cdot 10^{-2}$	$6.90 \cdot 10^{-1}$	14
E05	-0.0799	0.0814	0.1613	$-1.590 \cdot 10^{-4}$	$3.763 \cdot 10^{-2}$	$4.75 \cdot 10^{-1}$	13
E06	-0.1446	0.1469	0.2914	$1.125 \cdot 10^{-4}$	$6.022 \cdot 10^{-2}$	$1.92 \cdot 10^{-1}$	13
E07	-0.2075	0.1980	0.4055	$4.551 \cdot 10^{-5}$	$8.024 \cdot 10^{-2}$	$8.10 \cdot 10^{-2}$	14
E08	-0.2733	0.2739	0.5473	$-7.094 \cdot 10^{-5}$	$1.107 \cdot 10^{-1}$	$9.60 \cdot 10^{-1}$	14
E09	-0.2910	0.2787	0.5697	$5.784 \cdot 10^{-5}$	$1.037 \cdot 10^{-1}$	$6.12 \cdot 10^{-1}$	14
E10	-0.2954	0.2925	0.5879	$6.431 \cdot 10^{-5}$	$1.071 \cdot 10^{-1}$	$8.22 \cdot 10^{-1}$	14
E11	-0.1837	0.1991	0.3828	$1.190 \cdot 10^{-2}$	$8.393 \cdot 10^{-2}$	$4.03 \cdot 10^{-1}$	14
E12	-0.2117	0.2218	0.4335	$6.363 \cdot 10^{-5}$	$7.498 \cdot 10^{-2}$	$6.92 \cdot 10^{-1}$	14
E13	-0.2382	0.2376	0.4758	$-5.841 \cdot 10^{-7}$	$8.442 \cdot 10^{-2}$	$3.36 \cdot 10^{-1}$	14
E14	-0.2485	0.2339	0.4824	$-1.653 \cdot 10^{-3}$	$8.923 \cdot 10^{-2}$	$7.19 \cdot 10^{-2}$	14
E15	-0.2060	0.1813	0.3873	$-3.384 \cdot 10^{-4}$	$8.481 \cdot 10^{-2}$	$7.86 \cdot 10^{-1}$	14
E16	-0.2079	0.2044	0.4123	$5.221 \cdot 10^{-3}$	$8.084 \cdot 10^{-2}$	$6.83 \cdot 10^{-1}$	14
E17	-0.1373	0.1339	0.2712	$1.327 \cdot 10^{-4}$	$5.457 \cdot 10^{-2}$	$8.59 \cdot 10^{-1}$	13

At this point, it needs to be mentioned that the direct comparison of the seventeen filtered arrays of Ref. [1] and of the present study indicated that the impact of this modification on the important results would be insignificant.

3 The analysis of the filtered time-series arrays

Unlike in Ref. [1], all files will be allowed to enter the database in this work. This will be achieved as follows. The important results in a non-linear time-series analysis are obtained via iteration schemes over the input data. If the

time-series arrays are split into training and test sets, one file is chosen to become the source of embedding vectors at each iteration step (let me call this data set ‘test file’). By suitably using the embedding vectors obtained from the test file along with those contained in the database, one extracts estimates for the quantities which are relevant in non-linear analyses, e.g., for the optimal embedding dimension, for the correlation dimension, for the maximal Lyapunov exponent, etc. As aforementioned, the database was fixed in Ref. [1]. On the contrary, the database will be dynamically created in this work, comprising all available files, save the one chosen as test file at a given iteration step. The creation of such a dynamical database, depending on the choice of the input test file, enhances the statistics: it is expected to lead to a more reliable evaluation of the correlation sums $C(\epsilon)$ and of the out-of-sample prediction-error arrays $S(k)$, hence also of the estimates for the correlation dimension and for the maximal Lyapunov exponent.

Apart from the aforementioned modification, all details on the analysis of the filtered time-series arrays may be found in Ref. [1]. The maximal embedding delay of Table 1, namely $\nu = 14$, will be employed; the same value was also used in Ref. [1]. The results of this work will be obtained exclusively with the L^∞ distance: the distance between two vectors is defined as the maximal absolute difference between their corresponding components.

3.1 *Cao’s method for the determination of the optimal embedding dimension*

Cao’s quantities $E1$ and $E2$ were evaluated from the filtered time-series arrays for embedding dimensions up to $m = 15$, using (as the only input) $\nu = 14$. The results are shown in Fig. 1.

The results of the separate analysis² of the filtered data sets are shown in Fig. 2. There is general agreement between Figs. 1 and 2, and they both also agree with the corresponding plots of Ref. [1]. As in Ref. [1], $E1$ will be assumed to saturate in the vicinity of 10; in other words, $m_0 = 10$.

² To reduce the temporal correlations in the separate analysis of the data sets, all contributing (in the evaluation of $E1$ and $E2$) embedding vectors were required to have a temporal separation (constant distance between their corresponding elements) at least equal to the embedding delay $\nu = 14$. A minimal temporal separation of 150 $\Delta\tau$ (see Section 3.4) was also imposed on the data, but yielded similar results.

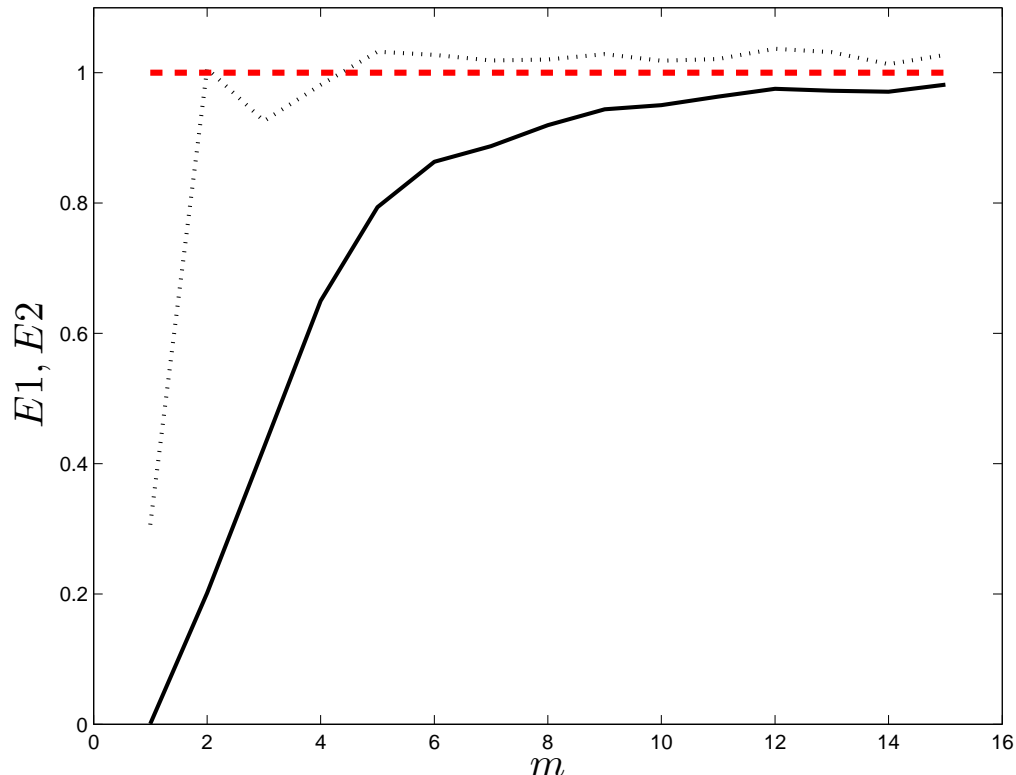


Fig. 1. Cao's $E1$ (straight line segments) and $E2$ (dotted line segments) for embedding dimensions m up to 15.

3.2 Correlation dimension

Introduced by Grassberger and Procaccia in 1983 [6], the correlation dimension is a measure of the dimensionality of the phase space of the system under study. It is obtained from the correlation sums $C(\epsilon)$, which represent the frequentness of embedding vectors in the time series whose distance does not exceed a given neighbourhood size ϵ . If no parts of the test files enter the database, the correlation sum $C(\epsilon)$ for embedding dimension m is defined in Eq. (8) of Ref. [1]. One is interested in the domain of neighbourhood sizes for which the relationship between $\ln C(\epsilon)$ and $\ln \epsilon$ is linear. Within that region,

$$\ln C(\epsilon) = \alpha \ln \epsilon + \beta , \quad (1)$$

where the slope α is identified with the quantity $\alpha(N, \epsilon)$ of Eq. (7) of Ref. [1]. At fixed m , the linearity between $\ln C(\epsilon)$ and $\ln \epsilon$ is investigated as in Ref. [1]: starting from the original $(\ln \epsilon, \ln C(\epsilon))$ points, the point with the largest ϵ value (one point per iteration) was removed, until the resulting p-value (obtained from the χ^2 value and the number of degrees of freedom in the linear fit,

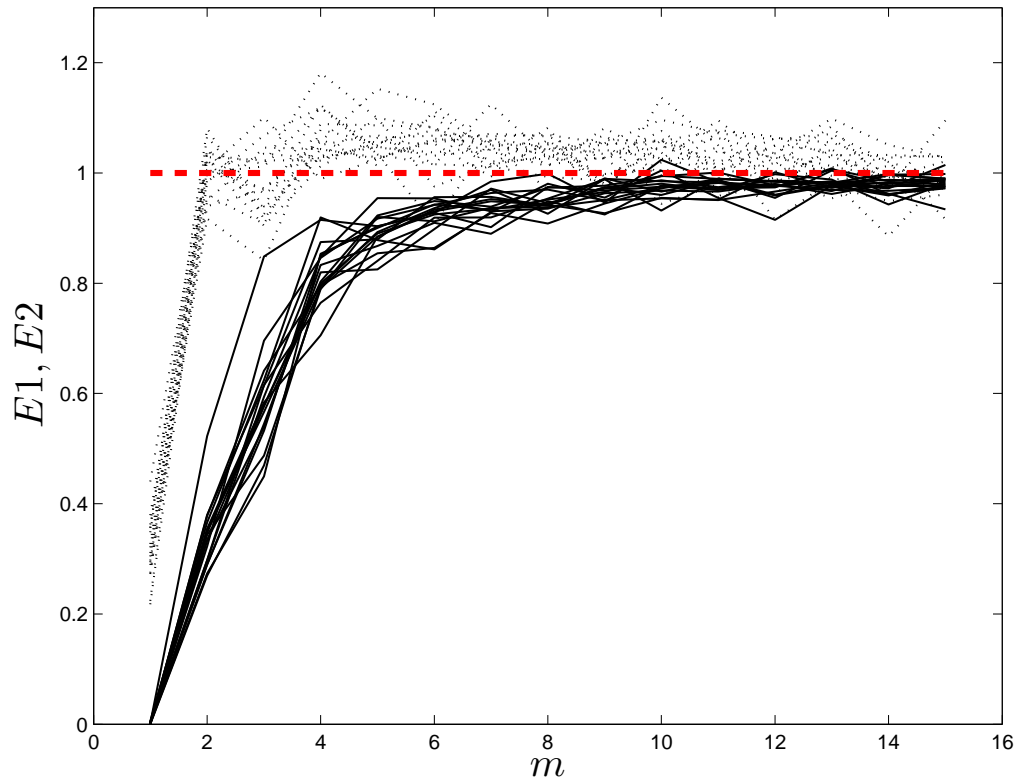


Fig. 2. Cao's $E1$ (straight line segments) and $E2$ (dotted line segments) for embedding dimensions m up to 15. These quantities were obtained from a separate analysis of the filtered time-series arrays. In order that their contributions to $E1$ and $E2$ be considered, the embedding vectors, involved in the evaluation, were required to have a temporal separation at least equal to $\nu\Delta\tau$.

see Ref. [1] for details) exceeded p_{\min} , the threshold of statistical significance. Evidently, the surviving $(\ln \epsilon, \ln C(\epsilon))$ points are those for which the linearity between $\ln C(\epsilon)$ and $\ln \epsilon$ is accepted at the assumed significance level.

To avoid the inclusion of noisy data in Ref. [1], a lower limit in the number of contributions was set in the evaluation of the correlation sums $C(\epsilon)$: points with fewer than $N_c = 10$ contributions to $C(\epsilon)$ were not considered. To investigate the stability of the results, it was decided to make use of four N_c values in this work: 10, 20, 50, and 100. The results for the extent of the linearity region and for the parameters of the linear fit, for these four N_c choices, are contained in Table 2.

Table 2

Results of the linear fits of Eq. (1) for embedding dimensions between 3 and 12. The given domain $[\epsilon_{\min}, \epsilon_{\max}]$ corresponds to the ϵ domain within which the linearity between $\ln C(\epsilon)$ and $\ln \epsilon$ is accepted ($p \geq p_{\min}$). The blocks correspond to four choices of N_c , i.e., of the lower number of neighbours for acceptable contributions in the evaluation of the correlation sums $C(\epsilon)$.

m	ϵ_{\min}	ϵ_{\max}	α	$\delta\alpha$	β	$\delta\beta$
$N_c = 10$						
3	$6.00 \cdot 10^{-3}$	$1.20 \cdot 10^{-2}$	2.9409	0.0055	6.612	0.025
4	$6.00 \cdot 10^{-3}$	$1.10 \cdot 10^{-2}$	3.900	0.018	9.561	0.083
5	$6.00 \cdot 10^{-3}$	$1.10 \cdot 10^{-2}$	4.828	0.040	12.50	0.18
6	$6.00 \cdot 10^{-3}$	$1.10 \cdot 10^{-2}$	5.893	0.081	16.08	0.37
7	$6.00 \cdot 10^{-3}$	$1.00 \cdot 10^{-2}$	7.41	0.32	21.9	1.5
8	$7.00 \cdot 10^{-3}$	$1.80 \cdot 10^{-2}$	6.645	0.045	17.06	0.18
9	$8.00 \cdot 10^{-3}$	$1.80 \cdot 10^{-2}$	7.479	0.089	19.58	0.37
10	$1.00 \cdot 10^{-2}$	$1.70 \cdot 10^{-2}$	9.09	0.26	25.3	1.1
11	$1.10 \cdot 10^{-2}$	$1.70 \cdot 10^{-2}$	10.10	0.51	28.5	2.1
12	$1.40 \cdot 10^{-2}$	$2.60 \cdot 10^{-2}$	8.661	0.072	21.69	0.27
$N_c = 20$						
3	$6.00 \cdot 10^{-3}$	$1.20 \cdot 10^{-2}$	2.9409	0.0055	6.612	0.025
4	$6.00 \cdot 10^{-3}$	$1.10 \cdot 10^{-2}$	3.900	0.018	9.561	0.083
5	$6.00 \cdot 10^{-3}$	$1.10 \cdot 10^{-2}$	4.828	0.040	12.50	0.18
6	$6.00 \cdot 10^{-3}$	$1.10 \cdot 10^{-2}$	5.893	0.081	16.08	0.37
7	$7.00 \cdot 10^{-3}$	$1.10 \cdot 10^{-2}$	6.89	0.18	19.42	0.82
8	$7.00 \cdot 10^{-3}$	$1.80 \cdot 10^{-2}$	6.645	0.045	17.06	0.18
9	$8.00 \cdot 10^{-3}$	$1.80 \cdot 10^{-2}$	7.479	0.089	19.58	0.37
10	$1.10 \cdot 10^{-2}$	$1.70 \cdot 10^{-2}$	9.02	0.26	25.0	1.1
11	$1.30 \cdot 10^{-2}$	$1.60 \cdot 10^{-2}$	10.8	1.1	31.6	4.5
12	$1.40 \cdot 10^{-2}$	$2.60 \cdot 10^{-2}$	8.661	0.072	21.69	0.27

From the entries of Table 2, one concludes that the dependence of the important results on N_c is weak; this is not a surprise, as the N_c cut affects only the points with the lowest ϵ values, hence those of the points which are accompanied by the largest statistical uncertainty. Using only sufficient embeddings

Table 2 continued

m	ϵ_{\min}	ϵ_{\max}	α	$\delta\alpha$	β	$\delta\beta$
$N_c = 50$						
3	$6.00 \cdot 10^{-3}$	$1.20 \cdot 10^{-2}$	2.9409	0.0055	6.612	0.025
4	$6.00 \cdot 10^{-3}$	$1.10 \cdot 10^{-2}$	3.900	0.018	9.561	0.083
5	$6.00 \cdot 10^{-3}$	$1.10 \cdot 10^{-2}$	4.828	0.040	12.50	0.18
6	$6.00 \cdot 10^{-3}$	$1.10 \cdot 10^{-2}$	5.893	0.081	16.08	0.37
7	$7.00 \cdot 10^{-3}$	$1.10 \cdot 10^{-2}$	6.89	0.18	19.42	0.82
8	$8.00 \cdot 10^{-3}$	$1.80 \cdot 10^{-2}$	6.638	0.045	17.03	0.19
9	$1.00 \cdot 10^{-2}$	$1.80 \cdot 10^{-2}$	7.464	0.095	19.52	0.39
10	$1.20 \cdot 10^{-2}$	$1.70 \cdot 10^{-2}$	8.95	0.30	24.7	1.2
11	$1.40 \cdot 10^{-2}$	$2.30 \cdot 10^{-2}$	8.285	0.087	21.01	0.34
12	$1.50 \cdot 10^{-2}$	$2.60 \cdot 10^{-2}$	8.640	0.068	21.61	0.25
$N_c = 100$						
3	$6.00 \cdot 10^{-3}$	$1.20 \cdot 10^{-2}$	2.9409	0.0055	6.612	0.025
4	$6.00 \cdot 10^{-3}$	$1.10 \cdot 10^{-2}$	3.900	0.018	9.561	0.083
5	$6.00 \cdot 10^{-3}$	$1.10 \cdot 10^{-2}$	4.828	0.040	12.50	0.18
6	$6.00 \cdot 10^{-3}$	$1.10 \cdot 10^{-2}$	5.893	0.081	16.08	0.37
7	$8.00 \cdot 10^{-3}$	$1.20 \cdot 10^{-2}$	6.41	0.18	17.19	0.81
8	$9.00 \cdot 10^{-3}$	$1.80 \cdot 10^{-2}$	6.635	0.049	17.02	0.20
9	$1.00 \cdot 10^{-2}$	$1.80 \cdot 10^{-2}$	7.464	0.095	19.52	0.39
10	$1.30 \cdot 10^{-2}$	$1.70 \cdot 10^{-2}$	8.84	0.36	24.2	1.5
11	$1.40 \cdot 10^{-2}$	$2.30 \cdot 10^{-2}$	8.285	0.087	21.01	0.34
12	$1.50 \cdot 10^{-2}$	$2.60 \cdot 10^{-2}$	8.640	0.068	21.61	0.25

($10 \leq m \leq 12$), one obtains for the slope α the values of 8.72 ± 0.15 , 8.69 ± 0.12 , 8.52 ± 0.13 , and 8.51 ± 0.12 for $N_c = 10, 20, 50$, and 100 , respectively. The estimate for the slope α , obtained in Ref. [1] for $N_c = 10$, was 8.830 ± 0.062 . One word about the increased uncertainties is due. In the approach followed in this work, the enhancement of statistics in the evaluation of the correlation sums $C(\epsilon)$ leads to smaller uncertainties $\delta \ln C(\epsilon)$, thus imposing more stringent conditions in the linear fits and, as it so happens, restricting the ϵ domain within which the linearity between $\ln C(\epsilon)$ and $\ln \epsilon$ is fulfilled. As a result, the estimates for the parameters of the linear fit are generally accompanied herein

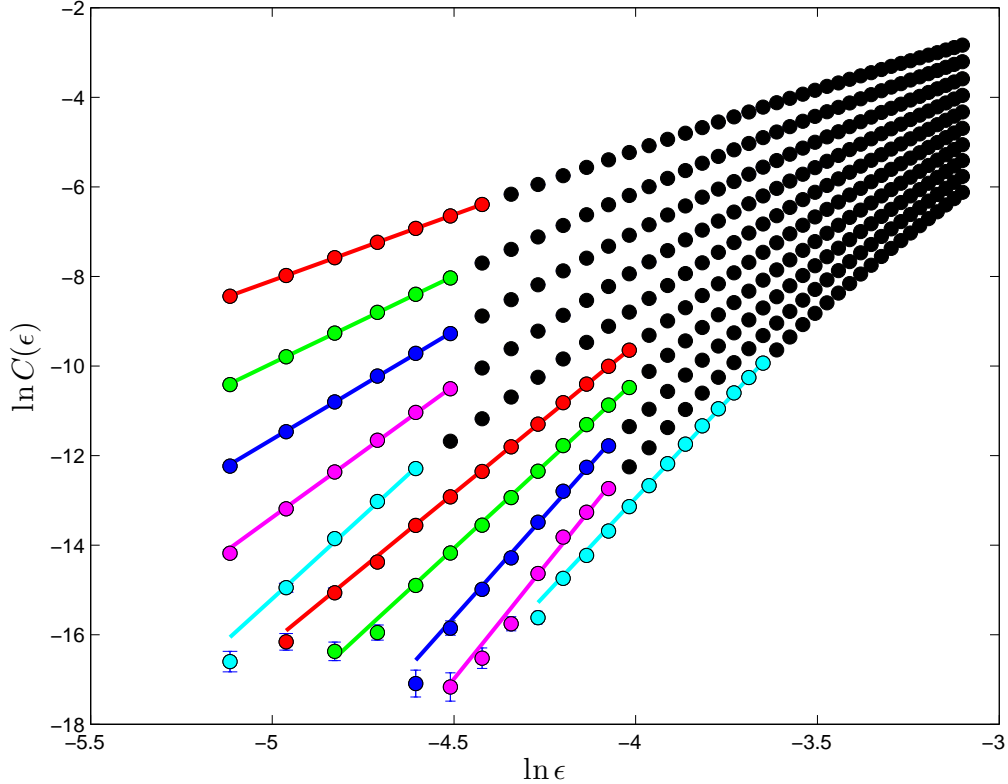


Fig. 3. The $(\ln \epsilon, \ln C(\epsilon))$ scatter plots for embedding dimensions $m = 3$ (top) to $m = 12$ (bottom). Weighted least-squares fits were performed on the data (see Table 2), separately for each embedding dimension, in the ϵ domain within which the linearity between $\ln C(\epsilon)$ and $\ln \epsilon$ holds (points and straight lines in colour); the data outside these ϵ domains are also shown (in black).

by larger fitted uncertainties (compared to those of Ref. [1]).

The estimates for the slope α agree within the uncertainties, and one does not have good reasons to depart from the choice $N_c = 10$ of Ref. [1]. Figures 3 and 4 contain the main results regarding the correlation dimension (for $N_c = 10$).

Before addressing the extraction of the maximal Lyapunov exponent, one word of caution is due. In this work, the contributions to the correlation sums $C(\epsilon)$ from two neighbouring vectors - belonging to two data sets, say, i and j - are bound to appear twice, once when the data set i is chosen to be the input test file and a second time when the data set j is selected. Provided that the quantities $C(\epsilon)$ are normalised, one might think that this ‘double counting’ is inessential. In reality, the $C(\epsilon)$ values do remain unchanged when using the complete database for each chosen test file (i.e., the embedding vectors constructed from all files, save the one chosen as test file at that iteration step),

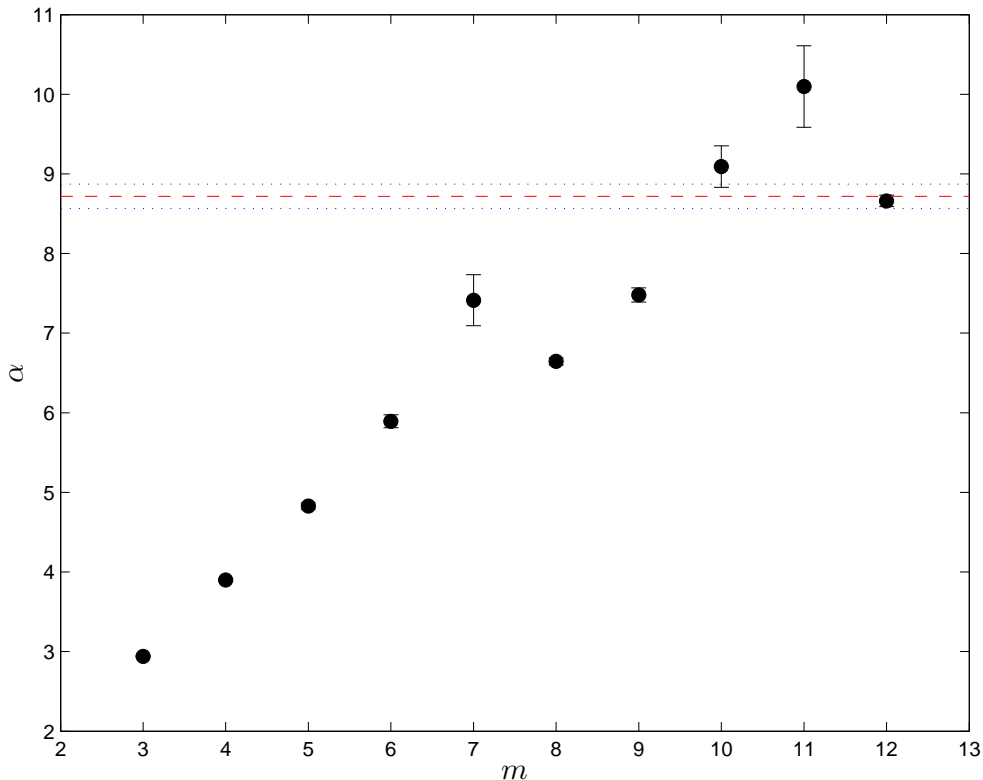


Fig. 4. The values of the slope α of the linear fits of Eq. (1). The red dashed line represents the weighted average over the α values for sufficient embeddings ($10 \leq m \leq 12$), see Table 2, block corresponding to $N_c = 10$. The blue dotted lines represent the 1σ limits of the statistical uncertainty, corrected for the quality of the reproduction of the three input α values by their weighted average. The slightly misplaced α value for $m = 11$ moves towards its two neighbours when larger N_c cuts are used, see Table 2.

yet their uncertainties (which are required in the test of linearity between $\ln C(\epsilon)$ and $\ln \epsilon$) are obviously affected. Therefore, when the iteration is made over all data sets and the database comprises all other files, one must bear in mind to take this ‘double counting’ into account in order to estimate $\delta \ln C(\epsilon)$ correctly. As a matter of fact, the implementation may be made in a clever way, avoiding this pitfall altogether; for instance, one may assume the order of Table 1 and allow only the data sets *after* the chosen test file to become part of the database corresponding to that input file.

3.3 Maximal Lyapunov exponent

The estimates for the maximal Lyapunov exponent were obtained as described in Section 5.6 of Ref. [1]. The out-of-sample prediction-error arrays $S(k)$ were evaluated using the appropriate variation of m and ϵ (i.e., within the linearity region in the $(\ln \epsilon, \ln C(\epsilon))$ scatter plots) and the distance-dependent weights $w_{ij} = 1 - (d_{ij}/\epsilon)^2$. Subsequently, their undulations were removed by fitting the monotonic function

$$S(k) = \ln \left[x_1 \exp \left[x_2 \left(1 + \frac{x_3}{x_1} \right) k \right] + x_3 \right] , \quad (2)$$

where the parameters $x_{1,2,3}$ are associated with the variation of $S(k)$ between $k = 0$ and saturation, the maximal Lyapunov exponent (λ), and the saturation level of $S(k)$, respectively; the expansion of $S(k)$ of Eq. (2) for small k values is: $S(k) \approx \ln(x_1 + x_3) + x_2 k$. The MINUIT package [7] of the CERN library (FORTRAN version) was used in the optimisation.

As in Ref. [1], the results of the fits with unreasonably large χ^2 values were removed after the application of a χ^2 cut, set equal to twice the median value of the original χ^2 distribution; 62 (out of the 81 original) fits with $\chi^2 \lesssim 264.23$ were accepted and yielded the maximal Lyapunov exponents shown in Fig. 5. The values, obtained for sufficient embeddings ($10 \leq m \leq 12$), were found compatible: the grand-mean value $\lambda = (8.9 \pm 0.7(\text{stat.}) \pm 1.9(\text{syst.})) \cdot 10^{-2} \Delta\tau^{-1}$ of this work is in very good agreement with the (slightly less precise) result of Ref. [1]: $\lambda = (9.2 \pm 1.0(\text{stat.}) \pm 2.7(\text{syst.})) \cdot 10^{-2} \Delta\tau^{-1}$. It should be reminded that the first uncertainty is statistical (average over fitted uncertainties, corrected for the quality of each fit), whereas the second one is systematic (reflecting the variation of λ with ϵ for the sufficient embeddings).

3.4 Space-time separation plot

I decided to include in this paper a few words on the widely-used space-time separation plot (STSP), whose visual inspection enables the extraction of an estimate for the temporal interval within which the elements of a given time series are (temporally) correlated. It has been known since a long time (e.g., see Ref. [8] and the references therein) that the temporal correlations affect the evaluation of the correlation sums $C(\epsilon)$, hence the determination of the estimate for the correlation dimension.

Despite the fact that no use of the STSP is called for herein, I will nevertheless concisely describe the method for the sake of completeness, and obtain results from the available data of PG 1159-035. Such information may be useful to

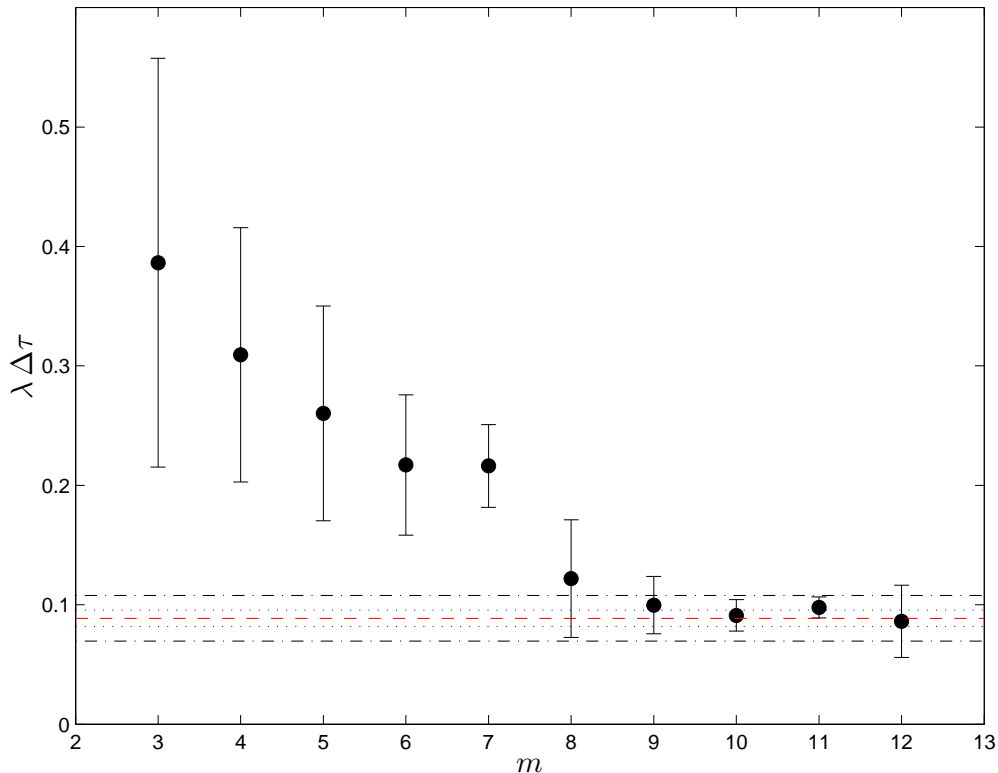


Fig. 5. The maximal Lyapunov exponents extracted from the filtered luminosity measurements of PG 1159-035 using Eq. (2). The sum of the statistical and systematic uncertainties is shown for each data point; the statistical uncertainties have been corrected for the quality of each fit. The red dashed line represents the grand mean over the ϵ values for sufficient embeddings ($10 \leq m \leq 12$). The blue dotted lines represent the 1σ limits of the statistical uncertainty of the grand mean, whereas the black dash-dotted lines correspond to the (1σ limits of the) systematic uncertainty.

those interested in including more of the available data in the dynamically-created database (and therefore need to fix n_{\min} in Eq. (6) of Ref. [1]).

For a time-series array comprised of independent elements, the probability $P(d_{ij} \leq \epsilon)$ (i.e., the probability that the distance d_{ij} between two embedding vectors i and j does not exceed a neighbourhood size ϵ) is expected to be only ϵ -dependent; it should not depend on the temporal separation Δt between the embedding vectors i and j . Therefore, if the percentiles of the d_{ij} distribution are plotted in 2 dimensions, i.e., as functions of ϵ (vertical axis) and of Δt (horizontal axis), the resulting curves should (in the absence of temporal correlations) be horizontal lines. On the contrary, if temporal correlations are present, a dependence of the percentiles of the d_{ij} distribution on Δt is un-

avoidable. To obtain an estimate for the minimal temporal separation between two elements of a time series, so that these elements be considered uncorrelated, Provenzale and collaborators [9] put forward the following procedure:

- fixation of Δt at several values,
- extraction of the d_{ij} distribution for embedding vectors separated by the chosen Δt value, and
- determination of the ϵ values corresponding to certain percentiles of the d_{ij} distribution (e.g., 10%, 20%, etc.) at the chosen Δt value.

The choice of the temporal interval which enables the mitigation/suppression of the effects of the temporal correlations simply reduces to the extraction (from the STSP) of the time above which the percentiles of the d_{ij} distribution are not dependent (at least, in a discernible way) on Δt .

The STSP, obtained from the available time-series arrays of PG 1159-035, is displayed in Fig. 6. An oscillatory pattern is seen, reflecting the periodicity of the input signal. (Another manifestation of this periodicity is the presence of undulations in the out-of-sample prediction-error arrays $S(k)$.) The STSP of PG 1159-035 is similar to the one obtained by Kantz and Schreiber [8] from the measurements of the flow of a viscous fluid between two coaxial cylinders (Taylor-Couette flow). In my opinion, a reasonable choice of n_{\min} would be 2–3 oscillation periods, i.e., $n_{\min} \approx 100–150$ (that is, about the optimal embedding window in this study); Kantz and Schreiber would probably recommend the use of an even larger n_{\min} value.

4 Discussion and conclusions

The goal in this work was the re-analysis of the luminosity measurements of the pre-white dwarf PG 1159-035, in fact those of the observations which found their way into the ‘Time-series data source Archives: Santa Fé time-series arrays Competition’ [2]. Two changes were implemented over the analysis of Ref. [1]:

- The original time-series arrays were subjected to a symmetrical, two-sided filtering procedure in this paper; on the contrary, the filtering was performed ‘left-to-right’ in Ref. [1]. The comparison of the filtered arrays between the two studies had indicated that the impact of this modification on the important results would not be significant.
- Unlike in Ref. [1], where the training and test sets were fixed at the outset of the study, the creation of a dynamical database, depending on the choice of the input test file, was employed in the present analysis. Given the substantial increase of the database (from Ref. [1] to this work), the significance of

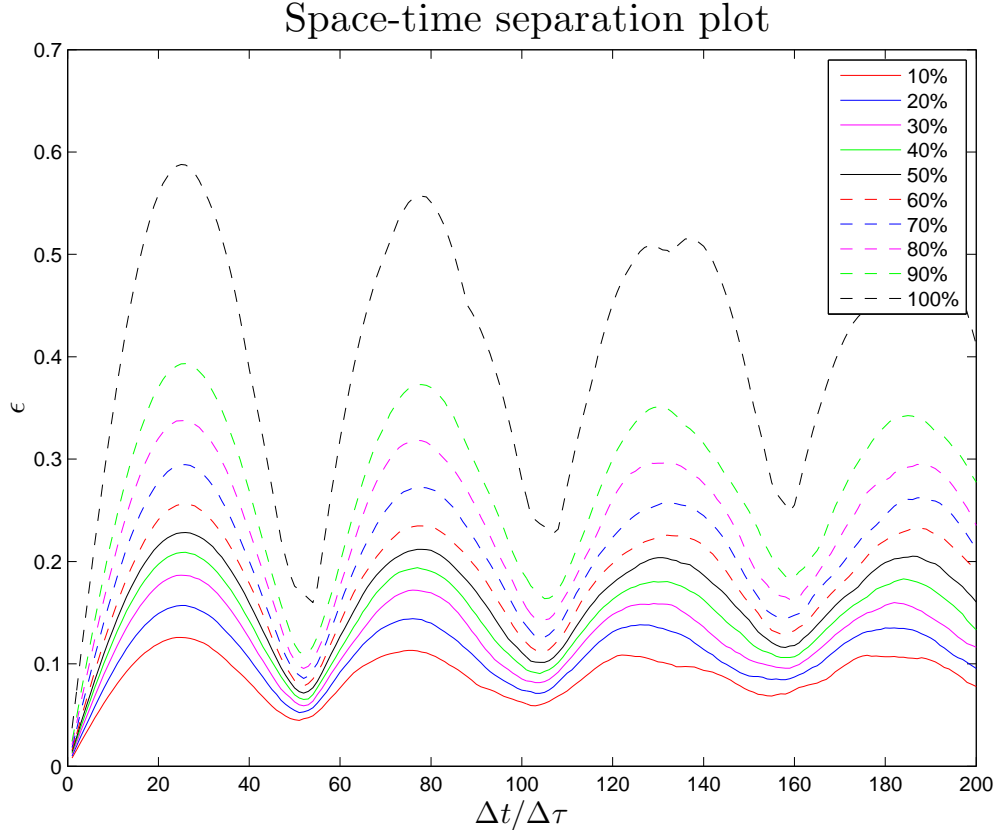


Fig. 6. The space-time separation plot corresponding to the filtered luminosity measurements of PG 1159-035: ϵ is the neighbourhood size and Δt is the temporal separation between two embedding vectors; the optimal embedding dimension $m_0 = 10$ was used in this plot. The values on the horizontal axis represent time steps in the original time-series arrays ($\Delta\tau = 10$ s). The curves correspond to different percentiles of the distribution of the distance between two embedding vectors (as detailed in the legend embedded in the plot).

this modification needed to be assessed.

The results of the analysis of the luminosity measurements of the pre-white dwarf PG 1159-035, obtained in this work, are similar to those reported in Ref. [1]. Evidently, the two aforementioned modifications do not affect the important results and the conclusions drawn in Ref. [1]. In particular, the maximal Lyapunov exponent λ , associated with the variation of the luminosity of PG 1159-035, came out equal to $(8.9 \pm 0.7(\text{stat.}) \pm 1.9(\text{syst.})) \cdot 10^{-2} \Delta\tau^{-1}$, in very good agreement with the result of Ref. [1]. ($\Delta\tau$ represents the sampling interval in the measurements, namely 10 s).

In relation to the subject of investigation in Ref. [1] and in the present work, I doubt that more information can be extracted from the luminosity measure-

ments of PG 1159-035 found in Ref. [2]. Although there is no indication that an enhanced database will lead to significant changes in the reported results, I will nevertheless express my interest again in receiving the complete data set of the 1989 runs from a credible source, e.g., directly from one of the members of the Whole Earth Telescope Collaboration.

Acknowledgements

All the figures were created with MATLAB [®] (The MathWorks, Inc., Natick, Massachusetts, United States).

References

- [1] E. Matsinos, ‘Analysis of luminosity measurements of the pre-white dwarf PG 1159-035’, [arXiv:1808.05132](https://arxiv.org/abs/1808.05132) [astro-ph.IM].
- [2] <http://www.comp-engine.org>
- [3] D.E. Winget et al., ‘Asteroseismology of the DOV star PG 1159-035 with the Whole Earth Telectope’, *Astrophys. J.* 378 (1991) 326–346. DOI: 10.1086/170434
- [4] J.E.S. Costa et al., ‘The pulsation modes of the pre-white dwarf PG 1159-035’, *Astron. Astrophys.* 477 (2008) 627–640. DOI: 10.1051/0004-6361:20053470
- [5] L. Cao, ‘Practical method for determining the minimum embedding dimension of a scalar time series’, *Physica D* 110 (1997) 43–50. DOI: 10.1016/S0167-2789(97)00118-8
- [6] P. Grassberger, I. Procaccia, ‘Measuring the strangeness of strange attractors’, *Physica D* 9 (1983) 189–208. DOI: 10.1016/0167-2789(83)90298-1
- [7] F. James, ‘MINUIT - Function Minimization and Error Analysis’, CERN Program Library Long Writeup D506.
- [8] H. Kantz, T. Schreiber, ‘Nonlinear Time Series Analysis’, Cambridge University Press, 1997; 2nd Edn., Cambridge University Press, 2004. ISBN: 0521821509, 0521529026
- [9] A. Provenzale, L.A. Smith, R. Vio, G. Murante, ‘Distinguishing between low-dimensional dynamics and randomness in measured time series’, *Physica D* 58 (1992) 31–49. DOI: 10.1016/0167-2789(92)90100-2